Mutational patterns and regulatory networks in epigenetic subgroups of meningioma

Nagarajan Paramasivam[1,2] · Daniel Hübschmann[1,3,4,5] · Umut H Toprak[6,7] · Naveed Ishaque[1,2,8] ·
Marian Neidert[9] · Daniel Schrimpf[10,11] · Damian Stichel[10,11] · David Reuss[10,11] · Philipp Sievers[10,11] ·
Annekathrin Reinhardt[10,11] · Annika K. Wefers[10,11] · David T. W. Jones[7,12,13,14] · Zuguang Gu[1,2] ·
Johannes Werner[1,15] · Sebastian Uhrig[16] · Hans-Georg Wirsching[17] · Matthias Schick[18] ·
Melanie Bewerunge-Hudler[18] · Katja Beck[2] · Stephanie Brehmer[19] · Steffi Urbschat[20] · Marcel Seiz-Rosenhagen[19] ·
Daniel Hänggi[19] · Christel Herold-Mende[21] · Ralf Ketter[20] · Roland Eils[1,8,22] · Zvi Ram[23,24] · Stefan M. Pfister[5,7,13] ·
Wolfgang Wick[25,26] · Michael Weller[17] · Rachel Grossmann[23,24] · Andreas von Deimling[10,11] · Matthias Schlesner[27] ·
Felix Sahm[7,10,11]

Abstract

DNA methylation patterns delineate clinically relevant subgroups of meningioma. We previously established the six meningioma methylation classes (MC) benign 1–3, intermediate A and B, and malignant. Here, we set out to identify subgroup-specific mutational patterns and gene regulation. Whole genome sequencing was performed on 62 samples across all MCs and WHO grades from 62 patients with matched blood control, including 40 sporadic meningiomas and 22 meningiomas arising after radiation (Mrad). RNA sequencing was added for 18 of these cases and chromatin-immunoprecipitation for histone H3 lysine 27 acetylation (H3K27ac) followed by sequencing (ChIP-seq) for 16 samples. Besides the known mutations in meningioma, structural variants were found as the mechanism of *NF2* inactivation in a small subset (5%) of sporadic meningiomas, similar to previous reports for Mrad. Aberrations of *DMD* were found to be enriched in MCs with *NF2* mutations, and *DMD* was among the most differentially upregulated genes in *NF2* mutant compared to *NF2* wild-type cases. The mutational signature AC3, which has been associated with defects in homologous recombination repair (HRR), was detected in both sporadic meningioma and Mrad, but widely distributed across the genome in sporadic cases and enriched near genomic breakpoints in Mrad. Compared to the other MCs, the number of single nucleotide variants matching the AC3 pattern was significantly higher in the malignant MC, which also exhibited higher genomic instability, determined by the numbers of both large segments affected by copy number alterations and breakpoints between large segments. ChIP-seq analysis for H3K27ac revealed a specific activation of genes regulated by the transcription factor FOXM1 in the malignant MC. This analysis also revealed a super enhancer near the *HOXD* gene cluster in this MC, which, together with general upregulation of *HOX* genes in the malignant MC, indicates a role of *HOX* genes in meningioma aggressiveness. This data elucidates the biological mechanisms rendering different epigenetic subgroups of meningiomas, and suggests leveraging HRR as a novel therapeutic target.

Nagarajan Paramasivam, Daniel Hübschmann, Matthias Schlesner, and Felix Sahm shared first or shared last authorship.

Introduction

Most meningiomas harbor alterations of *NF2*, with smaller subsets displaying mutations of *SMO*, *BAP1*, *SMARCE1*, *POLR2A*, *AKT1*, and *KLF4* (the last two mostly in combination with mutations of *TRAF7*) [5, 9, 10, 41, 47]. Also, mutations putatively cooperating with *NF2* loss have been

reported, resulting in higher malignancy, particularly in the *TERT* promoter and *ARID1A* [1, 26, 44]. On the basis of epigenetics, molecular subsets of meningioma can be identified [16, 38]. We recently devised a molecular approach to assist in the classification of meningioma employing DNA methylation profiling [45]. We identified six DNA methylation classes (MC): benign (ben) 1–3, intermediate (int) A and B, and malignant (mal). The three benign MCs have an outcome that is even more favorable than the average of WHO grade I cases, while cases of the malignant MC present with more rapid recurrence than the average anaplastic meningioma WHO grade III. The MCs are associated with distinct molecular alterations beyond DNA methylation: Most strikingly, MC ben-2 has a flat copy number profile and is virtually devoid of any *NF2* alterations but instead enriched for mutations in *AKT1*, *KLF4*, *TRAF7*, and *SMO*. The other MCs harbor chromosome 22q deletions and *NF2* mutations and accumulate further copy number alterations with increasing malignancy. For meningiomas arising after radiation (Mrad), often also referred to as "radiation-induced meningiomas," we previously showed that they harbor *NF2* alterations and DNA methylation profiles similar to sporadic *NF2*-altered meningiomas [46].

This molecular classification is particularly useful in identifying cases with inconspicuous histology but biological features of aggressive growth, and in turn also cases with criteria which already qualify for higher WHO grades but have biologically low risk of recurrence. Consequently, this approach has proven to significantly add to the risk prediction assessment compared to histology alone. Thus, it is already used to assist in the diagnostic workup for meningioma in select centers.

However, the full regulatory landscape, particularly of *NF2* mutant meningioma, rendering some low grade and others high grade on the basis of the same underlying mutation, is not fully understood. Further insight into the pathway activations distinguishing these clinically different subgroups may yield important insight for novel treatment approaches. To address these questions, we here set out to perform a comprehensive investigation of the genomic landscape and its relation to transcriptomic and epigenomic features of meningiomas across all WHO grades and MCs.

Materials and methods

Tissue of meningioma samples was acquired from the Dept. of Neurology Zürich (Switzerland), Dept. of Neurosurgery Homburg (Germany), Dept. of Neurosurgery Heidelberg (Germany), and the Tel Aviv Medical Center, Tel Aviv (Israel). Tissues were subjected to histopathological evaluation of the frozen section in order to ensure greater than 60% tumor cell content. In parallel, DNA was extracted from matched blood samples. DNA extraction was performed using the Promega Maxwell device. Samples were used in accordance with local ethical approval. Data on DNA sequencing of 17 Mrad was retrieved from a previous study [46]. Sample characteristics are depicted in Fig. 1a. Few samples had no accompanying information on WHO grade and the provided tissues were not suitable for full histopathological assessment and are therefore not assigned to a WHO grade. One case (sporadic_15) exhibited a very high number of single nucleotide variants (SNVs) during the subsequent pipeline of analyses (see below). Inspection of the patient's medical history revealed that the patient had developed acute myeloid leukemia (AML) previously and had received an allogenic bone marrow transplantation. Since this impedes the reliable classification of variants into somatic or germline and hence leads to a higher fraction of misclassified germline variants in the somatic calls, the patient has been excluded from the analysis of mutational load, mutational signatures, and genomic instability. Potentially, this meningioma could also have arisen in association with irradiation during therapy. Lacking further details about treatment, it was however termed "sporadic."

DNA methylation analysis

DNA methylation profiling of all samples was performed using the Infinium MethylationEPIC (850k) BeadChip (Illumina, San Diego, CA, USA) or Infinium HumanMethylation450 (450k) BeadChip (Illumina) array as previously described [45]. Filtering and genome-wide copy number analyses were performed as previously described, using the "conumee" package in R (https://www.bioconductor.org/packages/release/bioc/html/conumee.html) [49].

Whole genome sequencing (WGS)

DNA libraries were prepared according to the Illumina TruSeq Nano DNA Library protocol using the TruSeq DNA Nano kit (Illumina, Hayward, CA) and sequenced on two lanes on HiSeq X (2×151 bp) using the HiSeq X Ten Reagent Kit v2.5 (both Illumina, Hayward, CA).

Alignment and detection of small variants

The raw reads were mapped to the human reference genome (build 37, version hs37d5), using BWA mem (version 0.7.8, with parameter -T 0), sorted using SAMtools (version 0.1.19), and duplicate reads were marked using Picard (version 1.125, http://broadinstitute.github.io/picard). Using the tumor and corresponding matched normal samples, we called somatic small variants (SNVs and indels) using the in-house pipelines as described earlier [46]. Briefly, somatic SNVs were called using SAMtools mpileup (version
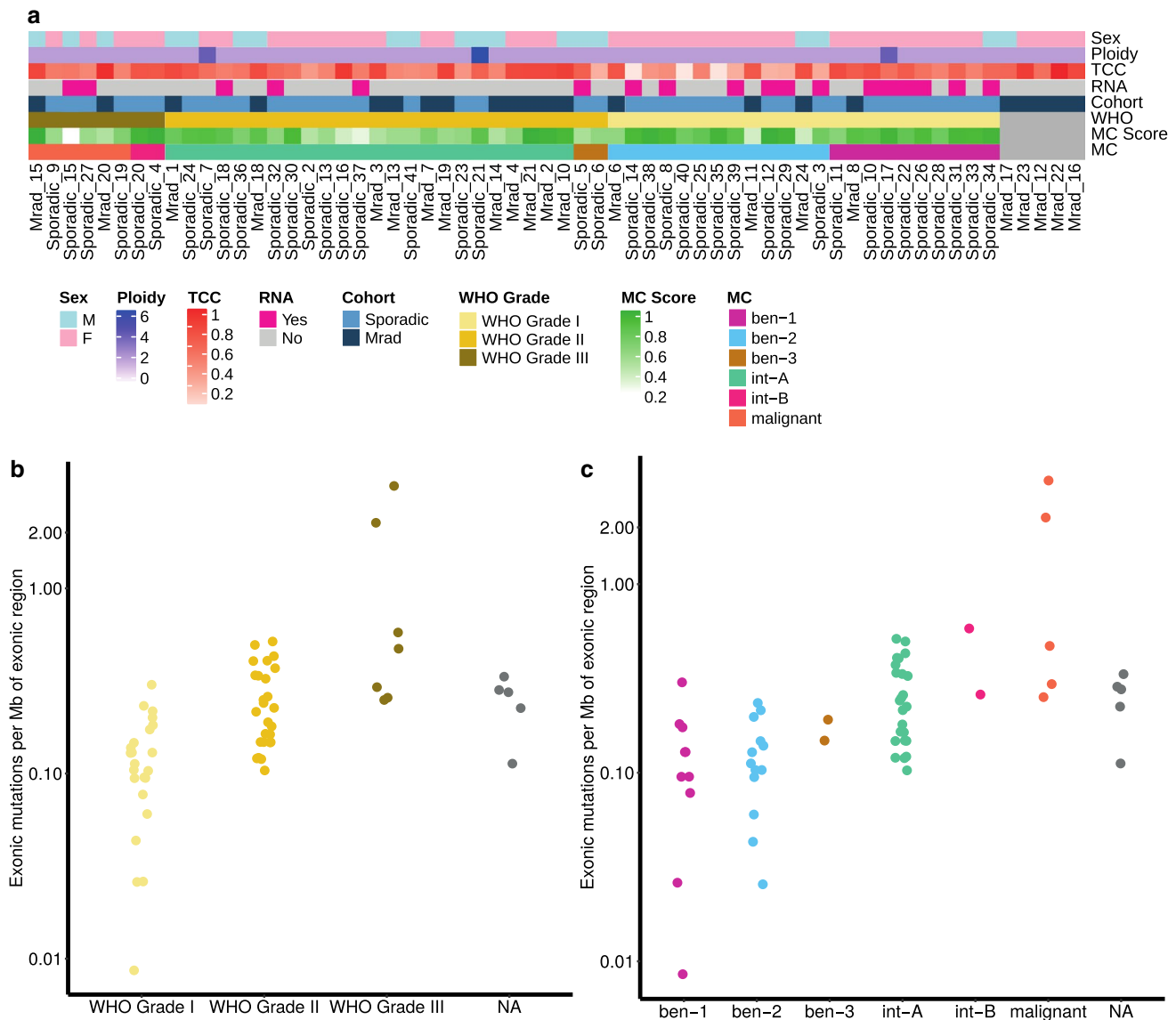
Fig. 1 a Characteristics of the cohort, sorted by meningioma methylation class (MC), with annotation of sex, ploidy, tumor cell content (TCC; ploidy and TCC were estimated from sequencing data using ACEseq), availability of RNA data, delineation of Mrad and sporadic cases, WHO grade, score for MC, and respective allocation to MC. Single nucleotide variants per coding megabase (Mb) stratified for WHO grade (**b**) and MCs (**c**). NA not available

0.1.19, with parameters -REI -q 30 -ug) and bcftools on tumor sample and then queried in the control samples (with parameters -ABRI -Q 0 -q 1). To enable calling of variants with low allele frequency we disabled the Bayesian model in bcftools (by setting -p 2). The raw calls were annotated with ANNOVAR and many publicly available tracks such as 1000 Genome variants, single nucleotide polymorphism database (dbSNP), genomic repeat and low complexity regions and locally available controls. Confidence scores for these variants were annotated as described previously [24]. Indels were called using Platypus (version 0.8.1, with parameters -bufferSize = 100,000 -maxReads = 5,000,000),

and were annotated similar to the somatic SNVs. High confidence somatic indels were required to have the genotype 0/0 (homozygous to reference allele) in the control sample and the platypus filter tag "PASS" or, to enable the detection of somatic variants with low allele frequency, pass custom filters when Platypus reported "allele bias." Somatic small variants present in ten or more samples in the local control list consisting of 280 WGS control samples from different cohorts, which were processed using the same pipelines, were considered as technical artifacts and were removed.

Somatic small variants misclassified as germline because of contamination of the matched normal samples with tumor

DNA/cells were rescued using the in-house tool TiNDA (Tumor in Normal Detection Analysis). Variant allele frequencies (VAFs) from variants which are classified as "germline" (i.e., variant reads have been identified in both tumor and the matched normal sample) and which are novel or rare (minor allele frequency (MAF) < 0.001 in gnomAD (version 2.0.1) and not present in the above local control list) were clustered using EM-based unsupervised clustering from Canopy (version 1.2.0) [23]. Clusters in which at least 85% of the members have a tumor VAF of at least 0.01 and a matched control VAF below 0.45 were considered as misclassified somatic variants. These rescued somatic SNVs and indels were mapped to the mpileup and Platypus raw calls and variants with confidence score greater than 7 were merged into the final somatic small variant calls. Variants in the remaining clusters were classified as rare germline and were annotated as rare high confidence germline variants if they had a confidence score greater than 7 in the corresponding raw calls.

Supervised and stratified analysis of mutational signatures

A supervised analysis of mutational signatures was performed with the R package YAPSA (Huebschmann et al. manuscript in preparation, https://bioconductor.org/packages/devel/bioc/html/YAPSA.html). The function `LCD_complex_cutoff()` in YAPSA was used to compute an NNLS decomposition of the mutational catalogue with the 30 known signatures from COSMIC (http://cancer.sanger.ac.uk/cosmic/signatures). To unambiguously identify the used signature set we denominate these signatures as AC1–AC30 (as abbreviation for Alexandrov COSMIC). YAPSA was also used for stratified analysis of mutational signatures in order to identify enrichment and depletion patterns. Breakpoint proximity was used as stratification axis with three strata: vicinity (distance to closest breakpoint < 100 kbp), intermediate (distance to closest breakpoint between 100 kbp and 1 Mbp), background (distance to closest breakpoint > 1 Mbp).

Structural variant detection

Genomic structural variants were detected using SOPHIA (version 34.0; https://bitbucket.org/utoprak/sophia) as described earlier [46], using a background population database consisting of 3216 WGS controls across different diseases (published TCGA cohorts and published/unpublished DKFZ cohorts) and sequencing technologies (100 bp read length Illumina HiSeq 2000/2500 and 151 bp read length Illumina HiSeq X) aligned using the same alignment settings and workflow as used in the present study. Gencode V19 was used for the gene annotations.

Copy number variation detection

Copy number states were called and tumor purity and ploidy were estimated using ACEseq (allele-specific copy number estimation from sequencing; https://www.biorxiv.org/content/early/2017/10/29/210807) as described previously [46]. In cases where ACEseq provides multiple purity and ploidy solutions, the lowest ploidy solution which allowed one to fit the majority of genomic segments to integer copy numbers and which was consistent with the mutant allele frequency distribution of somatic SNVs was manually selected.

Calculation of genomic instability scores

First, genome copy number data from ACEseq was smoothed to prevent artificially elevated genomic instability measures due to oversegmentation caused by technical noise. To this end, segments for which allele-specific copy numbers did not deviate by more than 0.3 from each other were merged. Furthermore, segments smaller than 3 Mb were merged to the more similar neighboring segment as previously described [2]. These smoothed segments were used to calculate the homologous recombination deficiency (HRD) score [2] and the number of large-scale transitions (LST) as previously described [39]. Briefly, segments larger than 15 Mb that were less than a whole chromosome in length and corresponded to a loss of heterozygosity were counted for the HRD score. For the quantification of LSTs, breaks between segments of different total copy number were counted with the constraint that both segments had to be larger than 10 Mb but did not correspond to entire chromosome arms. In addition, the telomeric-allelic imbalance (TAI) score [4] was calculated using the smoothed ACEseq results. Genomic instability was quantified as the sum of HRD, LST, and TAI scores.

Comparison of genomic instability score and methylation class

Differences in genomic instability scores between the different MCs were assessed by the Kruskal–Wallis test followed by post hoc pairwise Wilcoxon signed-rank tests. The R package ggpubr (version 0.1.6.999) was used to perform the tests and generate the plots.

RNA sequencing

RNAseq libraries were prepared using the Illumina TruSeq stranded mRNA kit and were sequenced on the Illumina HiSeq X Ten V2.5 platform. The paired-end reads were mapped to the STAR index generated reference genome (build 37, version hs37d5) using STAR (version 2.5.2b). Duplicate reads were marked using sambamba (version

0.4.6) and BAM files were coordinate sorted using SAMtools (version 1.19). featureCounts (version 1.5.1) was used to perform gene-specific read counting over exon features based on the gencode V19 gene model (without excluding read duplicates). Both reads of a paired fragment were used for counting and the quality threshold was set to 255 (which indicates that STAR found a unique alignment). Strandunspecific counting was used. For total library abundance calculations, during TPM expression values estimations, all genes on chromosomes X, Y, MT and rRNA and tRNA were omitted as they are likely to introduce library size estimation biases. Additionally, raw RNAseq reads from 32 formalin-fixed paraffin-embedded (FFPE) samples from the previous study used here for confirmatory analysis [45] were analyzed using the same data analysis pipeline. The TPM values from both cohorts were log2 transformed and standardized to *z*-scores [using the R code `scale(log2(TPMs_of_gene_in_cohort+0.000001))`] separately and then concatenated for comparisons and clustering analysis.

Gene fusion analysis

We extracted high-confidence gene fusion predictions from the chimeric alignments produced by STAR using our in-house pipeline Arriba (version 0.8, https://github.com/suhrig/arriba/), which removes recurrent alignment artifacts, transcript variants also observed in normal tissue, reads with low sequence complexity, and events with short anchors or breakpoints in close proximity or a low number of supporting reads relative to the overall number of predicted events in a gene [21].

Differential expression analysis

Differential expression (DE) of genes was analyzed using DESeq2 (version 1.14.1) [33]. DE analysis was performed with default settings in DESeq2 using raw read counts from featureCounts. Genes without any count in all samples were excluded from the analysis.

ChIP sequencing

Preparation for ChIP-seq was provided by ActiveMotif (Carlsbad, CA, USA). Immunoprecipitation was performed on 12 μg chromatin prepared from 200 mg of lysates from snap-frozen meningioma tissue with 4 μg anti-H3K27ac antibody 39133 at ActiveMotif. Three of the cases were also in the WGS cohort (Mrad_8, Mrad_12, sporadic_1); the other samples in the WGS cohort did not yield sufficient material. The other samples in the ChIP-seq cohort were selected from archival material based on availability of frozen tissue and in order to cover all MCs. No sufficient material was available for any ben-3 case. Thus, this MC

is not represented in the ChIP-seq analysis. Libraries were sequenced on the Illumina HiSeq 2000 platform V4. The raw paired-end reads were mapped to the human genome assembly (build 37, version hs37d5) using BWA mem v0.7.15 with default parameters. Duplicate marking was performed using Sambamba v0.6.5 with the following parameters: -t 1 -l 0 –hash-table-size = 2,000,000 –overflow-list-size = 1,000,000 –io-buffer-size = 64. ChIP-seq peaks from the sample BAM files were called against input DNA pool using MACS2 (version 2.1.1 [53]) with the following parameters: -f BAMPE -g hs -B -q 0.00001. ChIP-seq quality control was perfomed using the ChIPQC package (version 1.18.2) [6]. Quality control metrics including read length and library size are listed in Supplementary Table 4 (Online Resource 4).

Differential binding analysis

Differential peak binding was analyzed using DiffBind (version 2.10.0) [42]. The peak files were read in without the summit height detection option. Peaks that were present in at least two samples were used to generate the consensus peaks. DESeq 2 v1.22.2 via DiffBind was used for the differential analysis. Differential peak binding was tested for the samples of each methylation class (except Int-B) against the rest of all samples and for the combination of samples from two methylation classes against the rest of the samples (in total 14 tests for differential peak binding). In each test, peaks with a fold change of above three were considered as significant and a unique set of peaks from these 14 tests were used further.

A heatmap of the normalized peak counts from the significant peaks was generated using the R package ComplexHeatmap (version 1.99.0) [19]. ChIP-seq peaks (rows) were grouped into five clusters using *k*-means clustering (parameter row_km in the function Heatmap(); the seed was set to 42). Samples (columns) were subjected to a semi-supervised clustering using the MC information as group labels (parameter column_split in the function Heatmap()). The R package rGREAT (https://bioconductor.org/packages/release/bioc/html/rGREAT.html; version 1.14.0) was used to submit the significant peaks to the GREAT server [36] to perform pathway enrichment analysis with the MSigDB (Molecular Signature Database). Pathways with multiple testing-corrected (Benjamini Hochberg) *p* values less than 0.05 by binomial testing were considered as significant.

Transcription factor enrichment analysis

The HINT tool from the Regulator Genomics Toolbox (RGT, https://www.regulatory-genomics.org/hint/method/, version 0.11.4) was used to identify transcription factor footprints (TFF) in the MC-specific significant peaks on all samples separately. Overlapping TFF regions with more

than 20× coverage in all samples of an MC were selected for further analysis. These TFF regions were annotated for TF binding sites from the HOCOMOCO database using the MOTIF tool from RGT [30]. Enrichment of transcription factor binding sites in these TFF regions was evaluated by comparison to a set of random background regions (with the number of background regions being 10 times the number of input regions) using the MOTIF tool, as recommend by the RGT. As background regions, a random set of peak regions from the DiffBind consensus peaks were used.

Super enhancer analysis

Super enhancer (SE) analysis was performed using ROSE (Rank Ordering of Super-Enhancers) [34, 52] on the significant peaks from the malignant MC with the parameter -t 2500 (excludes regions ± 2.5 kb distance from RefSeq-annotated TSS in order to account for promoter biases). Super enhancers identified in at least two of the malignant samples were selected for further analysis.

The identified SE regions were visualized using the ChIP-seq profile plots from fluff (version 3.0.3) [17].

Driver analysis

Driver gene analysis using somatic SNVs and Indels was performed with IntOGen (version 3.0.5) [43] and MutSigCV (version 1.4) [32]. Firstly, significantly mutated genes or known cancer drivers as annotated by IntOGen that have mutations in two or more samples were considered as genes of interest (GOI). Second, for genes with more than two somatic functional small variants in a methylation class, we tested if mutations were significantly associated with the particular methylation class using the two-sided Fisher test and added genes with a *p* value less than 0.05 to the GOI list. Third, the top three genes with recurrent direct SVs (i.e., SVs with breakpoints in gene bodies) and the *TERT*, *LATS1*, *TFAP4*, and *ARID1B* genes were added to the above list. ComplexHeatmap was used to generate the oncoprint.

Data deposition

Data has been deposited at the European Genome-Phenome archive under the accession numbers EGAS00001003480 (ChiP-seq data) and EGAS00001003481 (WGS data).

Results

Mutations and structural variants in sporadic meningiomas and Mrad

We performed WGS on tumor tissue and matched blood to an average coverage of 79× from 62 patients with either sporadic meningiomas ($n = 40$) or Mrad ($n = 22$). DNA methylation profiling was performed for 57 and RNA sequencing for 18 cases (Fig. 1a). Finally, pathway activation was interrogated by chromatin-immunoprecipitation for H3K27Ac followed by sequencing on an additional 16 cases. We identified a median of 1657 somatic SNVs per case (range 123–25,274). The somatic mutational load, measured as the total number of somatic exonic mutations per Mb of exonic region, was higher in high-grade meningiomas (Fig. 1b). In line with this, stratification along the MCs revealed the lowest mutational load in the benign classes, a slightly increased mutational load in the intermediate classes, and the highest load in the malignant class (Fig. 1c).

Among the known meningioma-related genes, alterations in *NF2* (58%), *AKT1* (5%), *KLF4* (3%), *TRAF7* (10%), and *TERT* (5%, including two promoter mutations) were found (Fig. 2). WGS also allowed the identification of structural variants (SVs). Complete inactivation of the *NF2* gene product merlin was found to result not only from SNVs or small insertions/deletions (InDels) but also from SVs: While previously only reported for Mrad, we also detected SVs causing breakpoints in the *NF2* gene in two sporadic cases (5%). Two samples had *TERT* promoter hotspot mutations (indicated as upstream in Fig. 2) and one sample had a high amplification of the *TERT* gene body excluding the promoter. As expected, all but one samples classified as ben-2 were wild-type for *NF2* and samples of this MC were enriched for SNVs in *TRAF7*, *AKT1*, or *KLF4* (Supplementary Table 3, Online Resource 3). However, not all ben-2 cases harbored a mutation in one of these genes. While all *KLF4* mutations co-occurred with *TRAF7* mutations, we observed such co-occurrence with *KLF4* mutations only for one of three *AKT1* mutations. We identified *TFAP4* as an additional recurrently mutated gene in this MC; it was mutated in two ben-2 samples mutually exclusive to *TRAF7*, *AKT1*, and *KLF4*.

In addition, we found other genes recurrently altered by SNVs, indels, or SVs, most frequently *LRP1B* (15%), *PTPRD* (11%), and *DMD* (19%). Eleven out of 12 *DMD* mutant samples had *NF2* "double hits" through a combination of a chr22q deletion (including the gene *NF2*) and a mutation of *NF2*. Interestingly, the only remaining *DMD*-mutant sample harbored a deletion of chr6q where the gene *LATS1* is located and a somatic SNV affecting the
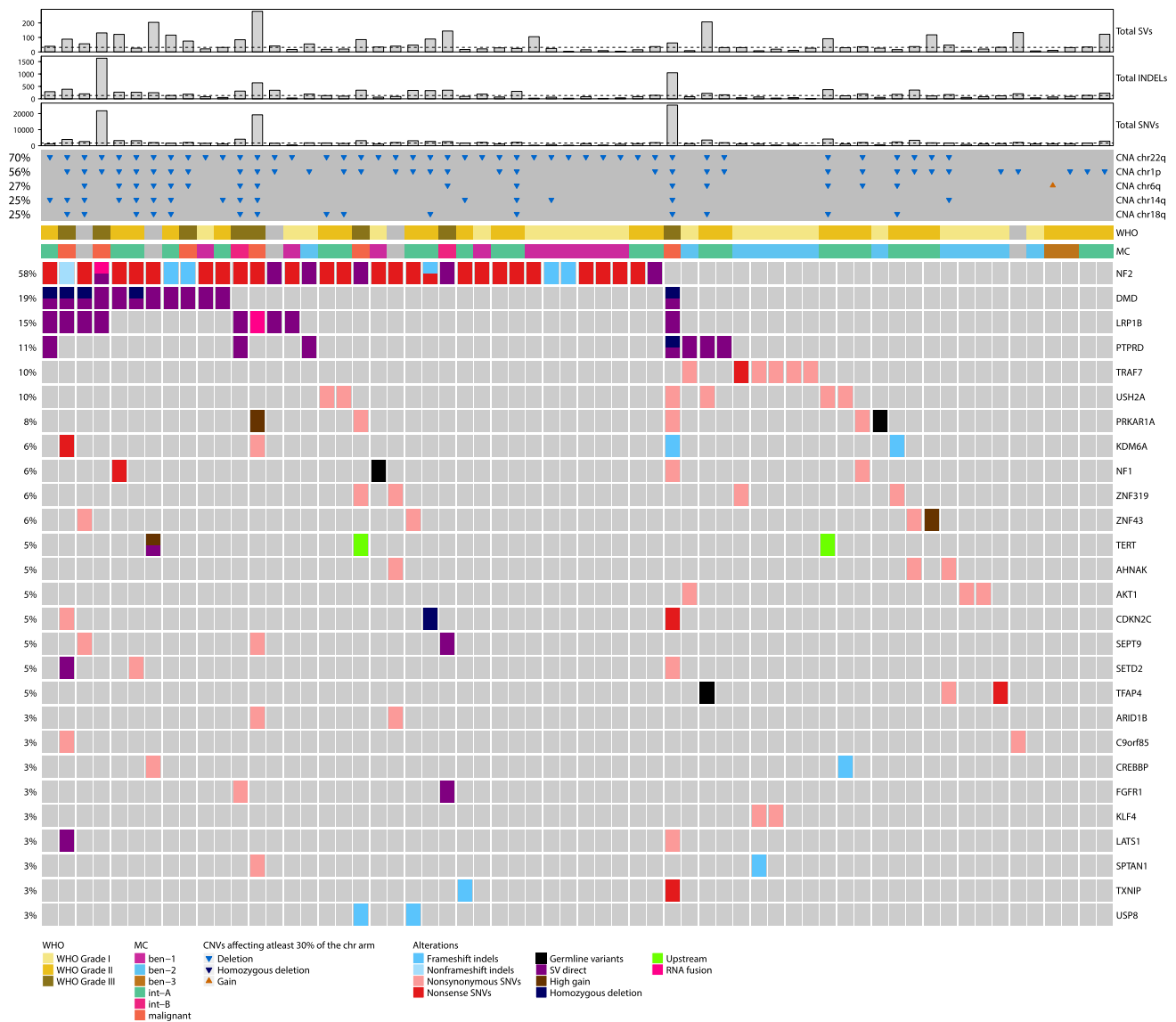
Fig. 2 Oncoprint of alterations found in the cohort. Annotations include the total number of structural variants (SVs), single nucleotide variants (SNVs), and small insertions/deletions (indels). Further, the most prevalent chromosomal alterations are provided, filtered for those affecting more than 30% of the chromosomal arm (complex alterations can lead to combined annotation of gain and loss if both events affect > 30% of the chromosomal arm). "Structural variants with breakpoints in the gene bodies are noted as "SV direct." For the *TERT* gene, SNVs in the promoter have been indicated as "Upstream". WHO grade and meningioma methylation class (MC) are also stated. The samples are hierarchically sorted by their mutation status in the indicated genes, starting with the most commonly affected gene, i.e., *NF2*. Genes are sorted by their alteration frequency

remaining *LATS1* allele. *LATS1* acts downstream of *NF2* in the Hippo signaling pathway, and its inactivation might hence provide an alternative mechanism of blocking the NF2 cascade [18, 37].

The large gene size of *DMD* (2.22 Mb) could point towards a non-significant "passenger" effect, which is further supported by its proximity to fragile sites on chromosome X. To further characterize the association between SVs in *DMD* and *NF2* mutations we investigated *DMD* expression levels in the methylation subgroups. *DMD* expression was higher in those subgroups typically harboring *NF2* mutations than in the *NF2* wild-type subgroup ben-2. This was observed in both the present cohort in which RNA of frozen tissue was used for sequencing and in RNA sequencing data generated from FFPE tissue retrieved from a previous study (Fig. 3a) [45]. Comparative assessment of *NF2* mutations and *DMD* status yielded that *NF2* mutant cases had higher *DMD* expression than *NF2* wild-type cases, while no association between *DMD* alteration status and *DMD* expression was apparent (Fig. 3b). Analysis of differentially expressed
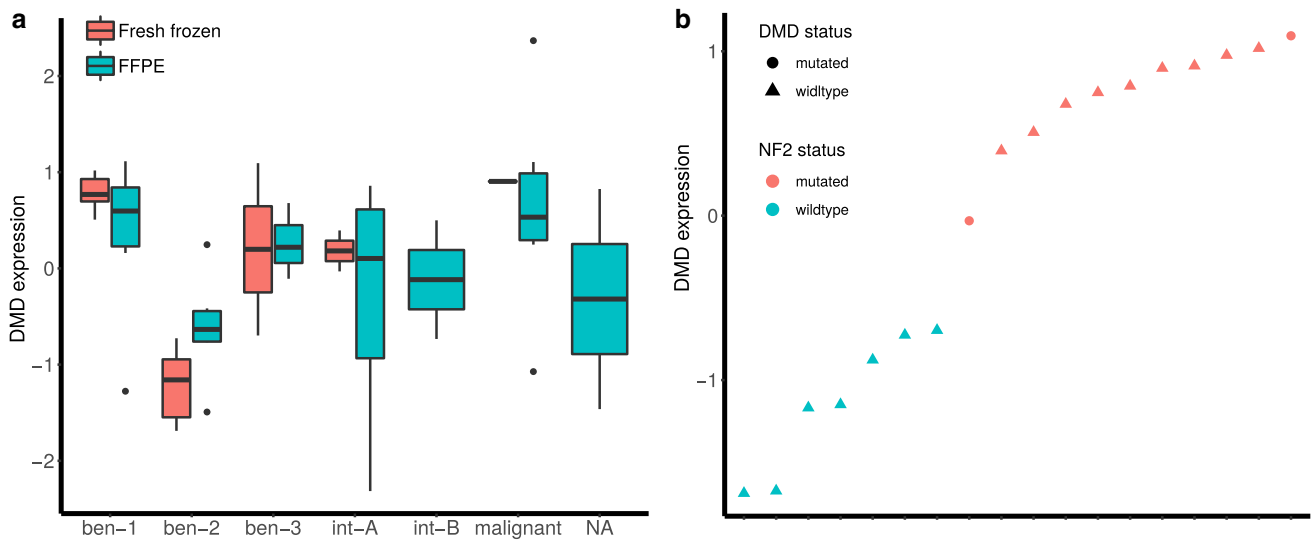
Fig. 3 **a** Expression of *DMD* in the cohort stratified for MC. In addition to the main cohort of this study (fresh frozen samples), previously generated data from FFPE tissue was also analyzed. Both batches show lower *DMD* expression in the MC ben-2 that typically is devoid of *NF2* alterations. **b** *DMD* expression in relation to *DMD* mutation status and *NF2* mutation status. "Mutated" indicates that the respective gene is affected by exonic SNVs or indels, or SVs with breakpoints in the gene body. *NF2* mutated samples showed higher *DMD* expression; *DMD* alterations occurred only in *NF2* mutant cases. Expression values are displayed as *z*-scores

genes between *NF2* wild-type and mutant cases revealed that *DMD* was among the most highly upregulated genes in *NF2* mutant cases (Supplementary Fig. 1, Online Resource 4).

Mutational signatures and genomic instability

We have previously described the presence of mutational signature AC3 in Mrad [46]. This mutational signature results from failure of double strand break repair by homologous recombination [3]. In Mrad, we had found that SNVs attributed to signature AC3 were enriched in the vicinity of breakpoints, which we could now confirm in additional Mrad cases in the present cohort (BH-corrected Kruskal–Wallis test $p = 0.014$). This finding led us to the hypothesis that this signature results from genomic rearrangements as a consequence of the irradiation [46]. Surprisingly, we identified in the current study a similar exposure (i.e., number of SNVs attributed to a mutational signature) to mutational signature AC3 in sporadic meningiomas (Supplementary Fig. 2, Online Resource 2). In contrast to Mrad, however, there was only a very slight non-significant enrichment of SNVs attributed to AC3 in the vicinity of breakpoints (Fig. 4a for Mrad and Fig. 4b for sporadic). To elucidate the origin of SNVs attributed to mutational signature AC3 in spontaneous meningiomas and to further characterize the differences between Mrad and spontaneous meningiomas, we tested if the absolute exposure to AC3 is correlated with genomic instability. Different measures of genomic instability have been established previously and have been shown to be associated

with defects in homologous recombination repair: (i) The number of deletions or loss of heterozygosity (LOH) events larger than 15 Mb, which has been termed the "homologous recombination deficiency score" (HRD score) [2]; (ii) The number of copy number changes between regions of at least 10 Mb in size denoted as large scale state transitions (LSTs) [39]; and (iii) The number of regions in allelic imbalance that extend to one of the subtelomeres of a chromosome, but do not cross the centromere, termed telomeric allelic imbalances (TAIs) [50]. As joint measure of genomic instability we have chosen the sum of HRD, LST, and TAI, calculated as described in Sect. "Calculation of genomic instability scores." This analysis revealed a significant correlation in sporadic meningiomas (Pearson's correlation test $p = 0.003$, $r = 0.47$), but not in Mrad (Pearson's correlation test $p = 0.27$, $r = 0.24$, Supplementary Fig. 3, Online Resource 4). Of note, AC3 is particularly enriched in meningiomas of the malignant MC (Fig. 4c), for which a high proliferative activity and high amounts of chromosomal alterations are typical. With the known correlation of large-scale chromosomal alterations being enriched in *NF2* mutant high-grade meningiomas, we investigated general differences in genomic instability between the MCs (Fig. 4d). Genomic instability was significantly higher in the malignant MC than in the low-grade *NF2* mutant ben-1 group (Wilcoxon $p = 0.003$) and in the low-grade *NF2* wild-type ben-2 group (Wilcoxon $p = 0.0011$). Altogether, these results indicate that both Mrad and sporadic meningiomas exhibit characteristics of a failure of HRR, but that the underlying cause might be different.
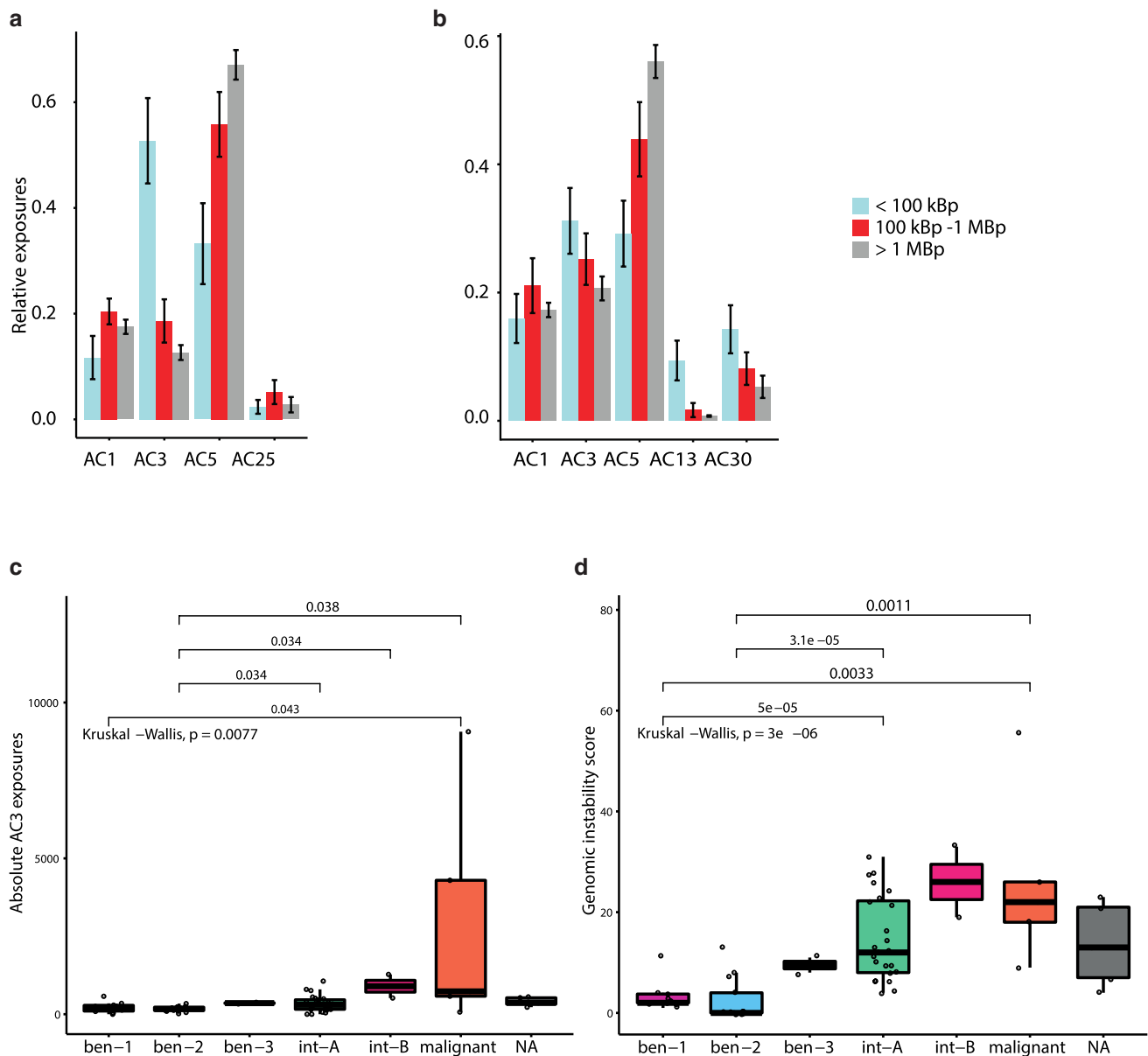
Fig. 4 Exposure to the most prevalent mutational signatures in Mrad (**a**) and sporadic meningiomas (**b**), stratified for distance to genomic breakpoints. Notably, AC3, associated with failure of homologous recombination repair and potential compensation by non-homologous end-joining repair, accumulates close to genomic breakpoints in Mrad but not in sporadic cases. The y-axis displays the relative exposures to the mutational signatures, i.e., the fraction of single nucleotide variants (SNVs) explained by the respective signatures. **c** Exposure to AC3 in the different MCs. AC3 is significantly enriched in the malignant MC. The y-axis displays the absolute exposures to the mutational signatures, i.e., the number of SNVs explained by the respective signatures. **d** General genomic instability is found in all high-grade MCs (int-A, B, malignant) and is lowest in the MC ben-2 which is predominantly *NF2*-wild-type. The genomic instability score on the y-axis displays the sum of the homologous recombination deficiency score, number of large-scale transitions score, and telomeric-allelic imbalance score (as explained in the main text)

Transcription factor recruitment

To further explore which molecular features distinguish the clinically different MCs we performed a comparative analysis of the epigenetic landscape by ChIP-seq of H3K27ac as active enhancer mark. A median of 61.85% of the reads per sample mapped to the identified peak regions; further quality control metrics are reported in Supplementary Table 4 (Online Resource 4). We identified 4566 unique peaks that exhibited differential binding between the MCs, which were grouped into five clusters using *k*-means clustering (Fig. 5a). Cluster 1 contained 1042 peaks which were specific for the malignant MC. Enrichment analysis using GREAT [36] and gene sets from MSigDB revealed
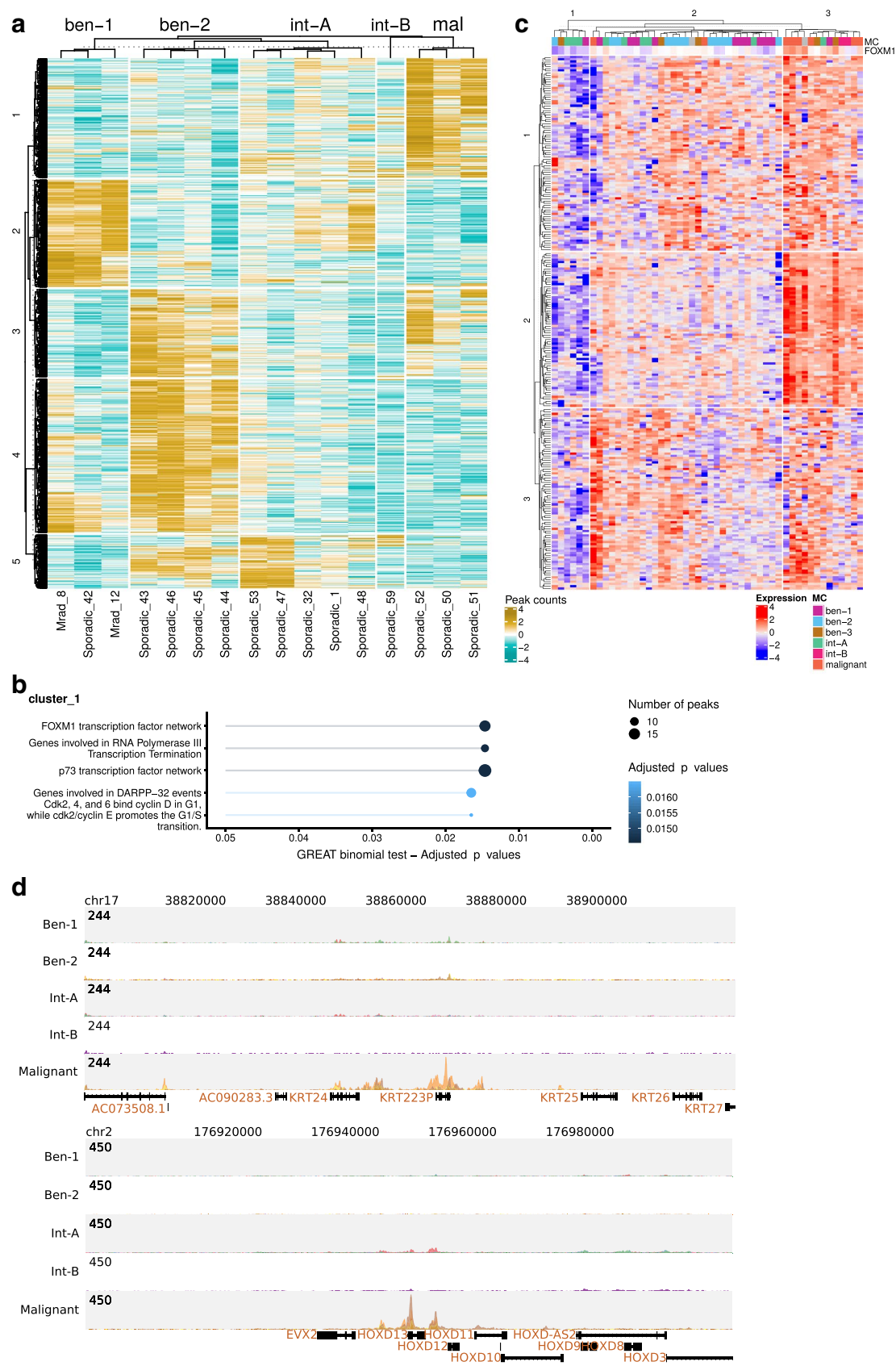
a

b

cluster_1

c

d

◀**Fig. 5 a** Heatmap of normalized count data from 4566 H3K27ac ChIP-seq peaks found to be significantly enriched in at least one MC. Columns were split on the basis of the MCs and rows were split by *k*-means clustering into five clusters. Cluster 1 contains peaks which are specific for the malignant MC. **b** Enrichment analysis of peaks from cluster 1 (i.e., peaks which are specific for the malignant MC) using GREAT and gene sets from MSigDB. The FOXM1 transcription factor network was found to be highly enriched among these peaks. The x-axis represents the corrected binomial *p* values, and the size represents the number of peaks/regions enriched for the corresponding gene set. **c** The expression of 240 FOXM1-regulated genes (source: genes near the ChIP-seq peaks identified in Chen et al.) [7] from 50 RNA-seq samples (18 fresh frozen and 32 FFPE samples) were clustered using *k*-means clustering and ordered using hierarchical clustering. *FOXM1* expression and MC classification were added as column annotations. Biologically more aggressive MCs, particularly the malignant MC cases, are enriched in cluster 3 in which *FOXM1* and FOXM1-regulated genes have higher expression. **d** ChIP-Seq profile plots for the super enhancer peaks in the keratin gene cluster on chromosome 17 and *HOXD* gene cluster on chromosome 2. The profiles are grouped on the basis of MCs

that among the peaks in cluster 1 genes from the FOXM1 transcription factor (TF) network were most highly enriched (Fig. 5b), indicating activation of FOXM1-regulated genes specifically in meningiomas from the malignant MC. In turn, clustering the expression for FOXM1-regulated genes revealed a cluster enriched with malignant MC cases, but also some lower grade cases (Fig. 5c). Motif enrichment analysis revealed enrichment of HOX genes among the peaks in cluster 1 (data not shown), and super enhancer (SE) analysis of these peaks additionally identified an SE in the HOXD cluster on chromosome 2 (Fig. 5d). In line with this, we observed increased expression of several *HOX* genes in the malignant samples (Supplementary Fig. 4, Online Resource 4). In addition, we observed SEs specific to the malignant MC within the keratin gene clusters (Fig. 5d) on chromosome 17 and in an established SE of *ADARB1* [27]. Overall, these findings imply that the transcription factor FOXM1 and several *HOX* genes contribute to malignancy of meningiomas.

Discussion

We here provide a multi-omics integrative analysis of sporadic meningiomas and meningiomas arising after radiation with data from WGS, RNA sequencing, and H3K27ac ChIP sequencing. Several previously established correlations between meningioma DNA methylation classes and genomic alterations were replicated, e.g., the low amount of *NF2* alterations in ben-2. In the other methylation classes *NF2* inactivation was common as expected, usually as a double hit with loss of one allele due to a large deletion on chr22 and an SNV or indel affecting the second allele. We have observed structural variations affecting

the *NF2* gene locus, including truncating gene fusions of *NF2*, in sporadic meningioma, which had so far only been reported in Mrad [5, 46]. This finding provides an explanation why some meningioma with the expected double hit could so far not be resolved by copy number assessment and exome sequencing alone and highlights the advantages of WGS analysis for understanding the pathogenetic mechanisms of tumors. Furthermore, we detected a double hit in *LATS1*, a gene downstream of *NF2* in the Hippo signaling pathway, in a case where no second hit of *NF2* was detectable. This suggests that *LATS1* inactivation might present a rare alternative mechanism to inactivate this pathway. Finally, we have found a copy number gain of the *TERT* locus as a potential alternative mechanism of *TERT* activation to promote meningioma growth in addition to *TERT* promoter mutations and the recently reported *TERT* fusions [25]. However, the *TERT* status was not related to telomerase expression or telomere length (not shown), similar to the findings from other recent studies [48].

In addition, WGS allowed the assessment of mutational signatures to investigate the mutational mechanisms which shaped the meningioma genomes. Our analysis revealed a difference between Mrad and sporadic meningiomas in the genomic distribution of mutational signature AC3, which is associated with failure of DNA double strand break repair by homologous recombination. Specifically, AC3 was strongly enriched close to genomic breakpoints in Mrad (Kruskal–Wallis test; corrected *p* value 0.014) but not significantly enriched in sporadic meningioma (Kruskal–Wallis test; corrected *p* value 0.660). These findings indicate a different origin of signature AC3 in Mrad and sporadic meningioma: In Mrad, AC3 most likely results from the repair of radiation-induced DNA double strand breaks by non-homologous end joining [35]. This may be due to an exhausted capacity of HRR at the loci of radiation-induced breakpoints and is hence enriched in the vicinity of these genomic breakpoints. In sporadic meningiomas, however, it might be a consequence of a constitutive repair deficiency, even if causative mutations in the homologous recombination repair pathway have not been detected. This is further supported by a correlation between AC3 exposure and genomic instability in sporadic meningioma but not in Mrad. According to our data, this instability is not only reflected by alterations of whole chromosomal arms as previously reported for high-grade *NF2* mutant meningiomas [20] but also finds a correlate at the level of sub-chromosomal events as quantified by HRD, LST, and TAI scores as well as SNV triplet patterns identified in mutational signature analysis. Importantly, genomic instability in combination with a high fraction of AC3 has previously been implicated as a BRCAness signature [8]. These findings on genomic instability and particularly a BRCAness signature might suggest the use

of PARP inhibitors in high-grade meningiomas similar to other entities with this pattern [13, 14, 29, 39].

The overall genomic instability may also be the cause of the high number of *DMD* SVs in *NF2* mutant cases, particularly of the malignant MC. The large gene size of *DMD* (2.22 Mb) could point towards a non-significant "passenger" effect, which is further supported by its proximity to fragile sites on chromosome X. The almost as frequently altered *LRP1B* gene is also located close to a fragile site, possibly indicating that these tumors are prone to SVs at fragile sites. Our data does not provide a clear proof for or against a specific functional role of *DMD* mutations in meningioma, and while the close correlation of *DMD* alterations and *DMD* expression with *NF2* mutations supports a distinct role in particularly *NF2* mutant cases, the high expression may also be associated with an open chromatin status with susceptibility to unselective mutations. A recent report by Juratli et al. found recurrent deletions of *DMD* in progressive or higher-grade meningioma [25], which also primarily affected exons 1 to 15, similar to our data set. They further investigated a potential functional and prognostic role of *DMD* in meningioma and found changes in the ultrastructural architecture of affected cells. They also identified an association of *DMD* deletions with progression and aggressive growth [25]. Thus, *DMD* could be valuable as an additional marker for identification of high-grade meningioma, which is also in line with our data. Gallia et al. found a very high prevalence of *DMD* deletions in olfactory neuroblastoma with 12 out of 14 investigated tumors being affected [15], which adds further evidence for a functional role of *DMD* in the development of certain tumors. Interestingly, also in the olfactory neuroblastoma predominantly exons towards the 5′ end of the gene were deleted, which might indicate that specifically deletion of this part of the gene while preserving the 3′ part confers an advantage during tumorigenesis. However, since in our data set only the 5′ exons of *DMD* were expressed in meningioma, it can also not be ruled out that the location of the deletion is the result of the underlying mutational mechanism which might be dependent on transcriptional activity [22]. Further studies are warranted to identify whether and how *DMD* loss contributes to development and aggressiveness of meningioma and if it may even represent a marker for sensitivity towards novel targeted therapies.

ChIP-seq analysis for H3K27ac as an active enhancer mark revealed an enrichment of *FOXM1* targets in peaks which are specific for meningiomas of the malignant MC, indicating a higher activity of the FOXM1 transcription factor in this MC. *FOXM1* has already been implicated in aggressive meningioma by previous studies [20, 31], and has most recently been proposed as a key transcription factor for meningioma proliferation [51]. Clustering of meningiomas according to the expression of *FOXM1* target genes revealed a cluster of high-grade cases but did not sharply dissect the MCs. The expression of these genes highly correlated with the expression of *FOXM1* itself.

We have found super enhancer activity specific for the malignant MC in the keratin gene cluster, the *HOXD* gene cluster, and near the *ADARB1* gene. The specific enhancer activity of *HOXD* is in line with several reports on deregulation of *HOX* genes in high-grade meningioma based on expression and DNA methylation data [11, 12, 16, 38], with the *HOXA* gene cluster being hypermethylated and the *HOXD* gene cluster being hypomethylated [28]. The strong activity of an SE cluster near *ADARB1* is consistent with differential methylation of this locus in aggressive meningiomas [38] and might pinpoint a role of RNA editing in driving malignancy in meningiomas. Of note, an association between high expression of *ADARB1* and decreased survival has previously been described in malignant mesothelioma [40].

Collectively, these data add to our understanding of what regulates meningioma growth and progression besides the underlying initiating mutations. In addition to the already implicated FOXM1 network, our findings of distinct mutational signatures being associated with the overall genomic instability of aggressive meningiomas may provide a novel target for therapies.

References

1. Abedalthagafi MS, Bi WL, Merrill PH et al (2015) ARID1A and TERT promoter mutations in dedifferentiated meningioma. Cancer Genet 208:345–350
2. Abkevich V, Timms KM, Hennessy BT et al (2012) Patterns of genomic loss of heterozygosity predict homologous recombination repair defects in epithelial ovarian cancer. Br J Cancer 107:1776–1782
3. Alexandrov LB, Nik-Zainal S, Wedge DC et al (2013) Signatures of mutational processes in human cancer. Nature 500:415–421
4. Birkbak NJ, Wang ZC, Kim JY et al (2012) Telomeric allelic imbalance indicates defective DNA repair and sensitivity to DNA-damaging agents. Cancer Discov 2:366–375
5. Brastianos PK, Horowitz PM, Santagata S et al (2013) Genomic sequencing of meningiomas identifies oncogenic SMO and AKT1 mutations. Nat Genet 45:285–289
6. Carroll TS, Liang Z, Salama R, Stark R, de Santiago I (2014) Impact of artifact removal on ChIP quality metrics in ChIP-seq and ChIP-exo data. Front Genet 5:75
7. Chen X, Muller GA, Quaas M et al (2013) The forkhead transcription factor FOXM1 controls cell cycle-dependent gene expression through an atypical chromatin binding mechanism. Mol Cell Biol 33:227–236

8. Chudasama P, Mughal SS, Sanders MA et al (2018) Integrative genomic and transcriptomic analysis of leiomyosarcoma. Nat Commun 9:144

9. Clark VE, Erson-Omay EZ, Serin A et al (2013) Genomic analysis of non-NF2 meningiomas reveals mutations in TRAF7, KLF4, AKT1, and SMO. Science 339:1077–1080

10. Clark VE, Harmanci AS, Bai H et al (2016) Recurrent somatic mutations in POLR2A define a distinct subset of meningiomas. Nat Genet 48:1253–1259

11. Collord G, Tarpey P, Kurbatova N et al (2018) An integrated genomic analysis of anaplastic meningioma identifies prognostic molecular signatures. Sci Rep 8:13537

12. Di Vinci A, Brigati C, Casciano I et al (2012) HOXA7, 9, and 10 are methylation targets associated with aggressive behavior in meningiomas. Transl Res 160:355–362

13. Engert F, Kovac M, Baumhoer D, Nathrath M, Fulda S (2017) Osteosarcoma cells with genetic signatures of BRCAness are susceptible to the PARP inhibitor talazoparib alone or in combination with chemotherapeutics. Oncotarget 8:48794–48806

14. Engert F, Schneider C, Weibeta LM, Probst M, Fulda S (2015) PARP inhibitors sensitize Ewing sarcoma cells to temozolomide-induced apoptosis via the mitochondrial pathway. Mol Cancer Ther 14:2818–2830

15. Gallia GL, Zhang M, Ning Y, Haffner MC, Batista D, Binder ZA (2018) Genomic analysis identifies frequent deletions of Dystrophin in olfactory neuroblastoma. Nat Commun. 9(1):5410

16. Gao F, Shi L, Russin J et al (2013) DNA methylation in the malignant transformation of meningiomas. PLoS One 8:e54114

17. Georgiou G, van Heeringen SJ (2016) fluff: exploratory analysis and visualization of high-throughput sequencing data. PeerJ 4:e2209

18. Godlewski J, Kiezun J, Krazinski BE, Koziolec Z, Wierzbicki PM, Kmiec Z (2018) The immunoexpression of YAP1 and LATS1 proteins in clear cell renal cell carcinoma: impact on patients' survival. Biomed Res Int 2018:2653623

19. Gu Z, Eils R, Schlesner M (2016) Complex heatmaps reveal patterns and correlations in multidimensional genomic data. Bioinformatics 32:2847–2849

20. Harmanci AS, Youngblood MW, Clark VE et al (2017) Integrated genomic analyses of de novo pathways underlying atypical meningiomas. Nat Commun 8:14433

21. Heining C, Horak P, Uhrig S et al (2018) NRG1 fusions in KRAS wild-type pancreatic cancer. Cancer Discov 8:1087–1095

22. Helmrich A, Ballarino M, Tora L (2011) Collisions between replication and transcription complexes cause common fragile site instability at the longest human genes. Mol Cell 44:966–977

23. Jiang Y, Qiu Y, Minn AJ, Zhang NR (2016) Assessing intratumor heterogeneity and tracking longitudinal and spatial clonal evolutionary history by next-generation sequencing. Proc Natl Acad Sci USA 113:E5528–5537

24. Jones DT, Hutter B, Jager N et al (2013) Recurrent somatic alterations of FGFR1 and NTRK2 in pilocytic astrocytoma. Nat Genet 45:927–932

25. Juratli TA, McCabe D, Nayyar N et al (2018) DMD genomic deletions characterize a subset of progressive/higher-grade meningiomas with poor outcome. Acta Neuropathol 136:779–792

26. Juratli TA, Thiede C, Koerner MVA et al (2017) Intratumoral heterogeneity and TERT promoter mutations in progressive/higher-grade meningiomas. Oncotarget 8:109228–109237

27. Khan A, Zhang X (2016) dbSUPER: a database of super-enhancers in mouse and human genome. Nucleic Acids Res 44:D164–171

28. Kishida Y, Natsume A, Kondo Y et al (2012) Epigenetic subclassification of meningiomas based on genome-wide DNA methylation analyses. Carcinogenesis 33:436–441

29. Kovac M, Blattmann C, Ribi S et al (2015) Exome sequencing of osteosarcoma reveals mutation signatures reminiscent of BRCA deficiency. Nat Commun 6:8940

30. Kulakovskiy IV, Vorontsov IE, Yevshin IS et al (2018) HOCOMOCO: towards a complete collection of transcription factor binding models for human and mouse via large-scale ChIP-Seq analysis. Nucleic Acids Res 46:D252–D259

31. Laurendeau I, Ferrer M, Garrido D et al (2010) Gene expression profiling of the hedgehog signaling pathway in human meningiomas. Mol Med 16:262–270

32. Lawrence MS, Stojanov P, Polak P, Kryukov GV et al (2013) Mutational heterogenieity in cancer and the search for new cancer genes. Nature. https://doi.org/10.1038/nature12213

33. Love MI, Huber W, Anders S (2014) Moderated estimation of fold change and dispersion for RNA-seq data with DESeq2. Genome Biol 15:550

34. Loven J, Hoke HA, Lin CY et al (2013) Selective inhibition of tumor oncogenes by disruption of super-enhancers. Cell 153:320–334

35. Mahaney BL, Meek K, Lees-Miller SP (2009) Repair of ionizing radiation-induced DNA double-strand breaks by non-homologous end-joining. Biochem J 417:639–650

36. McLean CY, Bristor D, Hiller M et al (2010) GREAT improves functional interpretation of cis-regulatory regions. Nat Biotechnol 28:495–501

37. Oh JE, Ohta T, Satomi K et al (2015) Alterations in the NF2/LATS1/LATS2/YAP pathway in Schwannomas. J Neuropathol Exp Neurol 74:952–959

38. Olar A, Wani KM, Wilson CD et al (2017) Global epigenetic profiling identifies methylation subgroups associated with recurrence-free survival in meningioma. Acta Neuropathol 133:431–444

39. Popova T, Manie E, Rieunier G et al (2012) Ploidy and large-scale genomic instability consistently identify basal-like breast carcinomas with BRCA1/2 inactivation. Cancer Res 72:5454–5462

40. Rehrauer H, Wu L, Blum W et al (2018) How asbestos drives the tissue towards tumors: YAP activation, macrophage and mesothelial precursor recruitment, RNA editing, and somatic mutations. Oncogene 37:2645–2659

41. Reuss DE, Piro RM, Jones DT et al (2013) Secretory meningiomas are defined by combined KLF4 K409Q and TRAF7 mutations. Acta Neuropathol 125:351–358

42. Ross-Innes CS, Stark R, Teschendorff AE et al (2012) Differential oestrogen receptor binding is associated with clinical outcome in breast cancer. Nature 481:389–393

43. Rubio-Perez C, Tamborero D, Schroeder MP, Antolín AA, Deu-Pons J, Perez-Llamas C et al (2015) In silico prescription of anticancer drugs to cohorts of 28 tumor types reveals novel targeting opportunities. Cancer Cell 27(3):382–96

44. Sahm F, Schrimpf D, Olar A et al (2016) TERT promoter mutations and risk of recurrence in meningioma. J Natl Cancer Inst 108:djv377

45. Sahm F, Schrimpf D, Stichel D et al (2017) DNA methylation-based classification and grading system for meningioma: a multicentre, retrospective analysis. Lancet Oncol 18:682–694

46. Sahm F, Toprak UH, Hubschmann D et al (2017) Meningiomas induced by low-dose radiation carry structural variants of NF2 and a distinct mutational signature. Acta Neuropathol 134:155–158

47. Smith MJ, O'Sullivan J, Bhaskar SS et al (2013) Loss-of-function mutations in SMARCE1 cause an inherited disorder of multiple spinal meningiomas. Nat Genet 45:295–298

48. Spiegl-Kreinecker S, Lotsch D, Neumayer K et al (2018) TERT promoter mutations are associated with poor prognosis and cell immortalization in meningioma. Neuro Oncol 20:1584–1593

49. Sturm D, Orr BA, Toprak UH et al (2016) New brain tumor entities emerge from molecular classification of CNS-PNETs. Cell 164:1060–1072

50. Telli ML, Timms KM, Reid J et al (2016) Homologous recombination deficiency (HRD) score predicts response to

platinum-containing neoadjuvant chemotherapy in patients with triple-negative breast cancer. Clin Cancer Res 22:3764–3773

51. Vasudevan HN, Braunstein SE, Phillips JJ et al (2018) Comprehensive molecular profiling identifies FOXM1 as a key transcription factor for meningioma proliferation. Cell Rep 22:3672–3683

52. Whyte WA, Orlando DA, Hnisz D et al (2013) Master transcription factors and mediator establish super-enhancers at key cell identity genes. Cell 153:307–319

53. Zhang Y, Liu T, Meyer CA et al (2008) Model-based analysis of ChIP-Seq (MACS). Genome Biol 9:R137

Affiliations

Nagarajan Paramasivam[1,2] · Daniel Hübschmann[1,3,4,5] · Umut H Toprak[6,7] · Naveed Ishaque[1,2,8] · Marian Neidert[9] · Daniel Schrimpf[10,11] · Damian Stichel[10,11] · David Reuss[10,11] · Philipp Sievers[10,11] · Annekathrin Reinhardt[10,11] · Annika K. Wefers[10,11] · David T. W. Jones[7,12,13,14] · Zuguang Gu[1,2] · Johannes Werner[1,15] · Sebastian Uhrig[16] · Hans-Georg Wirsching[17] · Matthias Schick[18] · Melanie Bewerunge-Hudler[18] · Katja Beck[2] · Stephanie Brehmer[19] · Steffi Urbschat[20] · Marcel Seiz-Rosenhagen[19] · Daniel Hänggi[19] · Christel Herold-Mende[21] · Ralf Ketter[20] · Roland Eils[1,8,22] · Zvi Ram[23,24] · Stefan M. Pfister[5,7,13] · Wolfgang Wick[25,26] · Michael Weller[17] · Rachel Grossmann[23,24] · Andreas von Deimling[10,11] · Matthias Schlesner[27] · Felix Sahm[7,10,11]

✉ Felix Sahm
felix.sahm@med.uni-heidelberg.de

1 Division of Theoretical Bioinformatics, German Cancer Research Center (DKFZ), Heidelberg, Germany

2 Heidelberg Center for Personalized Oncology (DKFZ-HIPO), German Cancer Research Center (DKFZ), Heidelberg, Germany

3 Division of Stem Cells and Cancer, DKFZ, Heidelberg, Germany

4 Heidelberg Institute for Stem Cell Technology and Experimental Medicine (HI-STEM gGmbH), Heidelberg, Germany

5 Department of Pediatric Oncology, Hematology and Immunology, University Hospital, Heidelberg, Germany

6 Division Neuroblastoma Genomics, German Cancer Research Center (DKFZ), Heidelberg, Germany

7 Hopp-Children's Cancer Center at the NCT Heidelberg (KiTZ), Heidelberg, Germany

8 Center for Digital Health, Berlin Institute of Health and Charité Universitätsmedizin Berlin, Berlin, Germany

9 Department of Neurosurgery, University Hospital of Zürich, Zurich, Switzerland

10 Department of Neuropathology, University Hospital Heidelberg, Im Neuenheimer Feld 224, 69120 Heidelberg, Germany

11 Clinical Cooperation Unit Neuropathology, German Consortium for Translational Cancer Research (DKTK), German Cancer Research Center (DKFZ), Heidelberg, Germany

12 Pediatric Glioma Research Group, German Consortium for Translational Cancer Research (DKTK), German Cancer Research Center (DKFZ), Heidelberg, Germany

13 Division of Pediatric Neurooncology, German Cancer Research Center (DKFZ), Heidelberg, Germany

14 German Cancer Consortium (DKTK), Heidelberg, Germany

15 Present Address: Department of Biological Oceanography, Leibniz Institute of Baltic Sea Research, Rostock, Germany

16 Division of Applied Bioinformatics, German Cancer Research Center (DKFZ), Heidelberg, Germany

17 Department of Neurology, University Hospital and University of Zurich, Zurich, Switzerland

18 Genomics and Proteomics Core Facility, Microarray Unit, German Cancer Research Center (DKFZ), Heidelberg, Germany

19 Department of Neurosurgery, University Hospital Mannheim, University of Heidelberg, Mannheim, Germany

20 Department of Neurosurgery, University Hospital Homburg Saar, Homburg, Germany

21 Division of Experimental Neurosurgery, Department of Neurosurgery, University Hospital Heidelberg, Heidelberg, Germany

22 Health Data Science Unit, Bioquant, Medical Faculty, University of Heidelberg, Heidelberg, Germany

23 Department of Neurosurgery, Tel Aviv Medical Center, Tel Aviv, Israel

24 Sackler School of Medicine, Tel Aviv University, Tel Aviv, Israel

25 Clinical Cooperation Unit Neurooncology, German Cancer Consortium (DKTK), German Cancer Research Center (DKFZ), Heidelberg, Germany

26 Department of Neurology and Neurooncology Program, National Center for Tumor Diseases, Heidelberg University Hospital, Heidelberg, Germany

27 Bioinformatics and Omics Data Analytics, German Cancer Research Center (DKFZ), Heidelberg, Germany